

Ion-induced electron production in tissue-like media and DNA damage mechanisms

E. Surdutovich^{1,2a}, O. I. Obolensky^{1,5}, E. Scifoni¹, I. Pshenichnov^{1,3}, I. Mishustin^{1,4}, A. V. Solov'yov^{1,5b}, and W. Greiner¹

¹ Frankfurt Institute for Advanced Studies, Ruth-Moufang-Str. 1, 60438 Frankfurt am Main, Germany

² Department of Physics, Oakland University, Rochester, Michigan 48309, USA

³ Institute for Nuclear Research, Russian Academy of Science, 117312 Moscow, Russia

⁴ Kurchatov Institute, Russian Research Center, 123182 Moscow, Russia

⁵ *On leave from A.F. Ioffe Physical-Technical Institute, 194021 St. Petersburg, Russia*

Received: March 3, 2008 / Revised version: date

Abstract. We propose an inclusive approach for calculating characteristics of secondary electrons produced by ions/protons in tissue-like media. This approach is based on an analysis of the projectile's interaction with the medium on the microscopic level. It allows us to obtain the energy spectrum and abundance of secondary electrons as functions of the projectile kinetic energy. The physical information obtained in this analysis is related to biological processes responsible for the irreparable DNA damage induced by the projectile. In particular, we consider double strand breaks of DNA caused by secondary electrons and free radicals, and local heating in the ion's track. The heating may enhance the biological effectiveness of electron/free radical interactions with the DNA and may even be considered as an independent mechanism of DNA damage. Numerical estimates are performed for the case of carbon-ion beams. The obtained dose-depth curves are compared with results of the MCHIT model based on the GEANT4 toolkit.

PACS. 61.80.-x Physical radiation effects, radiation damage – 87.53.-j Effects of ionizing radiation on biological systems – 41.75.Ak Positive-ion beams – 34.50.Bw Energy loss and stopping power

1 Introduction

Ion and proton beams are becoming more and more popular tools for cancer therapy. Ions and protons are more advantageous projectiles than the now conventional photons because they may cause less damage to the healthy tissues surrounding tumors and thus induce fewer side effects. More details on the history, current status and comparison of proton and heavy-ion therapies can be found in the review articles [1,2,3,4].

The method of radiation therapy consists in the inactivation of cancer cells via radiation impact on their DNA [5]. The DNA may be destroyed in a number of ways [6]. Double strand breaking (DSB) is one of the most effective mechanisms of irreparable DNA damage. Interactions of low-energy secondary electrons and free radicals with the DNA are believed to be mainly responsible for the DSB's [7]. We are going to build an inclusive approach yielding such microscopic characteristics as abundance of secondary electrons and free radicals in the region as well as their energy spectrum. These characteristics can be obtained from the analysis of the interaction of projectiles

with the medium. We hope that this approach will facilitate establishing a quantitative connection between the amount of energy deposited into the tissue and the induced biological consequences. Another mechanism that we discuss in this paper is the DNA damage due to local heating of the medium.

Regardless of the eventual mechanism of the DNA damage, a projectile's propagation and stopping is the basic process in cancer therapy and therefore we start our study with its analysis. All secondary electrons and free radicals that may cause DNA damage as well as the medium's temperature increase are due to energy loss by these projectiles. For numerical estimates, we have taken parameters characteristic of cancer radiation therapy using carbon-ion beams.

When an energetic charged projectile enters a medium, it experiences a number of atomic and nuclear interactions. Nuclear processes, mainly fragmentation reactions, result in the transformation of the beam particles into new species. The nuclear processes can be reliably modeled with the use of Monte-Carlo simulations, in particular by means of the MCHIT model [8,9,10] based on the GEANT4 toolkit [11,12]. Therefore in this paper, we only comment on projectile fragmentation processes without

^a *E-mail: surdutov@oakland.edu; Tel: +1-248-370-3409*

^b *E-mail: solovyov@fias.uni-frankfurt.de*

considering them in detail. Atomic processes, such as elastic Coulomb scattering, scattering with excitation, single and multiple ionization, are much more probable but less destructive events for the projectile, frequently occurring along the projectile's trajectory. Ionization of molecules of the target media is the main channel of the projectile's energy loss. This process is the most important for biological applications since it results in a shower of secondary electrons, which may inflict more DNA damage than the projectile itself.

In Section 2, we study the passage of a single ion through the medium, analyze the impact ionization cross section, linear energy transfer (LET), and evaluate the abundance of secondary electrons and their energy spectrum. Calculations are carried out for parameters typical for cancer therapy. They are compared with experimental results and the predictions of the MCHIT model for the depth-dose distributions. In Section 3, we estimate the densities of electrons and free radicals produced by the projectiles. Finally, we evaluate the local heating associated with the energy loss, and estimate DNA damage due to thermal effects.

2 Ion passage through the medium

We first describe the passage of a single ion through biological medium. The medium is approximated by liquid water, which, anyhow, is the major component of most living tissues. The ion typically enters the medium with a sub-relativistic velocity (the corresponding energy range used in carbon-ion therapy is 100–400 MeV per nucleon) and then gradually slows down because of energy loss in inelastic processes. As mentioned above, the impact ionization is the dominant energy-loss process. Most importantly, this process results in the production of secondary electrons, which are directly or indirectly responsible for the radiation damage of DNA.

The inelastic cross sections are smaller at the beginning of the trajectory (at high velocities) but then increase and reach a maximum at the so-called Bragg peak. In the vicinity of this maximum, the ion loses its energy at the highest rate. As its velocity decreases further, the cross section drops because of kinematic constraints.

In our first analysis [13], we have limited our consideration to non-relativistic projectile velocities. However, the relativistic effects are significant for 400 MeV/u ions, and in this work, we include relativistic corrections. As shown below, this results in better agreement of our calculations with the measured position of the Bragg peak.

Emission of electrons (frequently called δ -electrons) in proton collisions with atoms and molecules has been under theoretical and experimental investigation for decades [14,15]. The quantity of interest is the probability to produce N secondary electrons with kinetic energy W , in the interval dW , emitted from a segment Δx of the trajectory of a single ion at the depth x corresponding to the kinetic energy of the ion, T , within the solid angle $d\Omega$. This quantity is proportional to the doubly-differentiated cross section

(DDCS)

$$\frac{d^2 N(W, T)}{dW d\Omega} = n \Delta x \frac{d^2 \sigma(W, T)}{dW d\Omega}, \quad (1)$$

where n is the number density of water molecules (at standard conditions $n \approx 3.3 \times 10^{22} \text{cm}^{-3}$).

In our current analysis, the angular distribution of emitted electrons is not important, therefore we integrate over the solid angle and the DDCS is replaced with a single-differential cross section (SDCS). Thus, the total impact ionization cross section, differentiated in secondary electron kinetic energy, $d\sigma(W, T)/dW$, becomes the main quantity in our analysis. Besides the kinetic energy of secondary electrons and the properties of water molecules, the SDCS depends on the kinetic energy of the projectile T and its charge z . We use the semi-empirical Rudd's expression [15] for the SDCS, which is a parametric adjustment that combines the experimental data, calculations within the plane wave Born approximation and other theoretical models. It is given in the following form [15]:

$$\frac{d\sigma(W, T)}{dW} = z^2 \sum_i \frac{4\pi a_0 N_i}{I_i} \left(\frac{R}{I_i}\right)^2 \times \frac{F_1(v_i) + F_2(v_i)\omega_i}{(1 + \omega_i)^3 (1 + \exp(\alpha(\omega_i - \omega_i^{\max})/v_i))}, \quad (2)$$

where the sum is taken over the electron shells of the water molecule, $a_0 = 0.0529 \text{ nm}$ is the Bohr radius, $R = 13.6 \text{ eV}$ is the Rydberg, N_i is the shell occupancy, I_i is the ionization potential of the shell, $\omega_i = W/I_i$ is the dimensionless normalized kinetic energy of the ejected electron, v_i is the dimensionless normalized projectile velocity given by

$$v_i = \sqrt{\frac{mV^2}{2I_i}}, \quad (3)$$

where m is the mass of electron and V is the velocity of the projectile. In the non-relativistic case, the expression (3) is the square root of the kinetic energy of an electron having the same velocity as the projectile, normalized by the corresponding binding energy. The definition of v_i remains in the relativistic case, however, the projectile velocity V is no longer equal to $\sqrt{\frac{2T}{M}}$ (where M is the mass of a projectile), but is rather given by βc , where $\beta^2 = 1 - 1/\gamma^2 = 1 - (Mc^2/(Mc^2 + T))^2$, and γ is the Lorentz factor of the projectile.

Furthermore, F_1 and F_2 in (3) are given by

$$F_1(v) = A_1 \frac{\ln(1 + v^2)}{B_1/v^2 + v^2} + \frac{C_1 v^{D_1}}{1 + E_1 v^{D_1+4}}, \quad (4)$$

and

$$F_2(v) = C_2 v^{D_2} \frac{A_2 v^2 + B_2}{C_2 v^{D_2+4} + A_2 v^2 + B_2}. \quad (5)$$

The corresponding fitting parameters taken from Ref. [15], $A_1 \dots E_1, A_2 \dots D_2, \alpha$ are listed in tables I and II. The

Table 1. Fitting parameters for the three outer shells of water molecule with the ionization potentials $I_1 = 12.61$ eV, $I_2 = 14.73$ eV, $I_3 = 18.55$ eV.

A_1	B_1	C_1	D_1	E_1	A_2	B_2	C_2	D_2	α
0.97	82	0.4	-0.3	0.38	1.04	17.3	0.76	0.04	0.64

Table 2. Fitting parameters for two inner shells of water molecule with the ionization potentials $I_4 = 32.2$ eV, $I_5 = 539.7$ eV

A_1	B_1	C_1	D_1	E_1	A_2	B_2	C_2	D_2	α
1.25	0.5	1.0	1.0	3.0	1.1	1.3	1.0	0.0	0.66

cut-off energy ω^{\max} is given by

$$\omega_i^{\max} = 4v_i^2 - 2v_i - \frac{R}{4I_i}, \quad (6)$$

where the first term on the right hand side represents the free-electron limit, the second term represents a correction due to electron binding, and the third term gives the correct dependence of the SDCS for $v \ll 1$ [15]. For $v \gg 1$, Rudd's formula would have the correct relativistic asymptotics if F_1 , given by (4), is replaced by the following expression,

$$F_1(v) = A_1 \frac{\ln\left(\frac{1+v^2}{1-\beta^2}\right) - \beta^2}{B_1/v^2 + v^2} + \frac{C_1 v^{D_1}}{1 + E_1 v^{D_1+4}} \quad (7)$$

whose asymptotic behaviour is clearly similar to the well known Bethe-Bloch formula for energy loss:

$$-\frac{dT}{dx} \sim \frac{1}{\beta^2} \left[\ln\left(\frac{2mc^2\beta^2}{\langle I \rangle (1-\beta^2)}\right) - \beta^2 \right], \quad (8)$$

where $\langle I \rangle$ is the average ionization potential for water molecule. This correction reveals itself as an increase of the cross section at high energies. In our calculations, we omitted the term $-\beta^2$ in the numerator of Eq. (7) after checking its negligible contribution in the energy range of interest. The SDCS for water as a function of the projectile's and secondary electron's energies is plotted in Fig. 1.

In our previous consideration [13], the charge of the projectile, z , which enters into the expression (3) was taken to be constant and equal to the charge of a fully stripped projectile nucleus. This led to a prediction of unphysically large heights of the Bragg peak in disagreement with experimental data. This indicates that the charge transfer, or electron capture by a charged projectile, takes place in the vicinity of the Bragg peak, effectively reducing the charge of the projectile [17]. Therefore, z in (3) should be replaced by an effective charge z_{eff} which decreases with decreasing energy making the cross section effectively smaller. In this work, we use z_{eff} given by Barkas [18] which represents the average ion charge at a given ion velocity βc :

$$z_{eff} = z(1 - \exp(-125\beta z^{-2/3})). \quad (9)$$

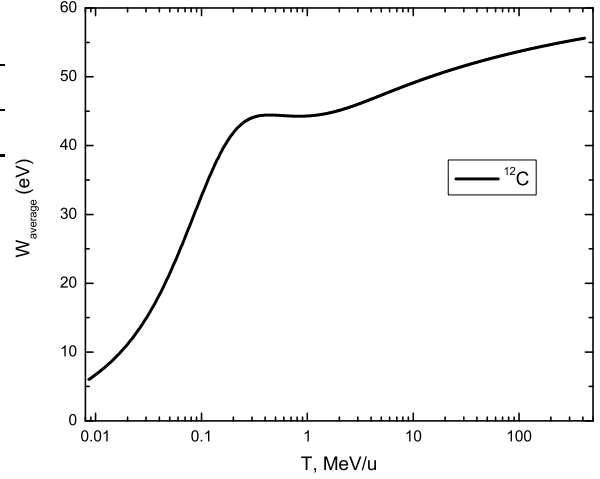


Fig. 2. Average energy of secondary electrons produced as the result of impact ionization as a function of kinetic energy of $^{12}\text{C}^{6+}$ ions.

The effective charge given by this expression slowly changes at high projectile velocity, but rapidly decreases in the vicinity of the Bragg peak. As a result, the charge transfer does not affect the position of a Bragg peak, but it may significantly affect its height.

Integration of the singly-differentiated cross section over secondary electron energy W gives the total cross section of impact ionization by the ion with the kinetic energy T :

$$\sigma(T) = \int_0^\infty \frac{d\sigma(W, T)}{dW} dW. \quad (10)$$

This quantity is important for all our calculations. Infinity as the upper limit of the integration in this and other expressions that follow is not physical, but still appropriate because of the exponential factor in denominator of (3), which effectively truncates the integral, [15].

The next characteristic that we can obtain from the SDCS is the average energy of the secondary electrons, which is given by

$$W_{ave}(T) = \frac{1}{\sigma(T)} \int_0^\infty W \frac{d\sigma(W, T)}{dW} dW. \quad (11)$$

The result of this integration is shown in Fig. 2. It is worth noting that on the average, the secondary electrons are not very energetic, about 50-60 eV, and the average energy levels out as the energy of the projectile increases. This fact is important for estimating the probability of avalanches initiated by the first generation of emitted electrons.

The stopping cross section, defined as

$$\sigma_{st} = \sum_i \int_0^\infty (W + I_i) \frac{d\sigma_i(W, T)}{dW} dW, \quad (12)$$

gives the average energy lost by a projectile in a single collision, which can be further translated into energy loss

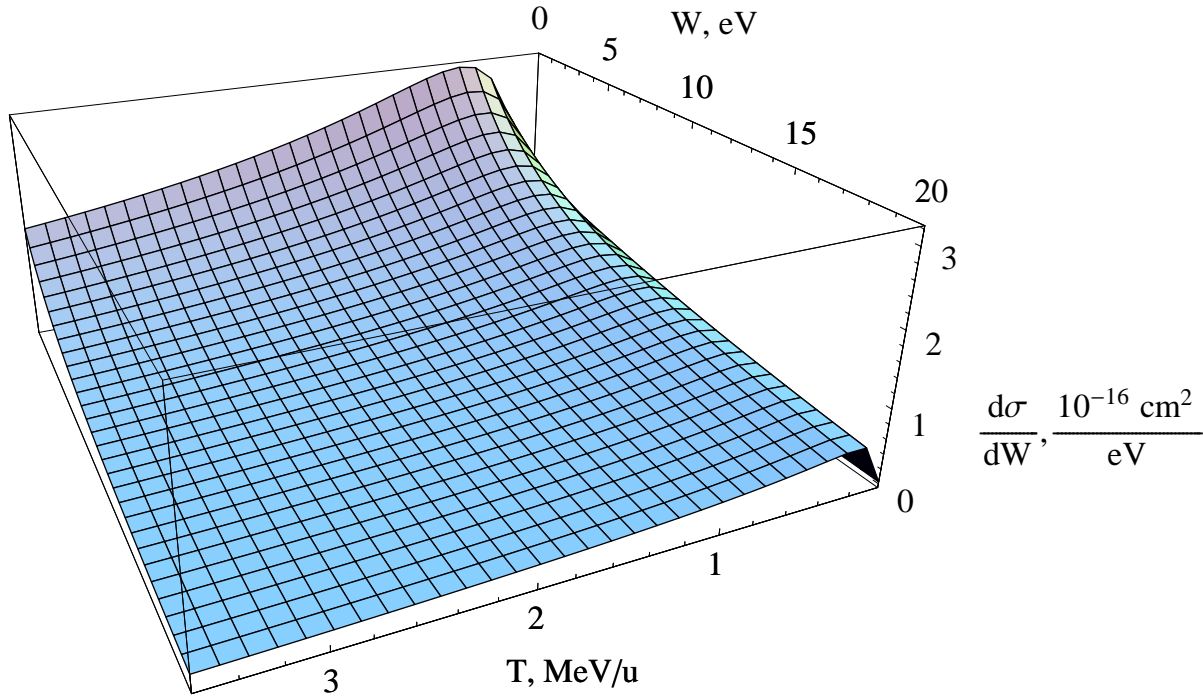


Fig. 1. Singly differentiated ionization cross section for ions $^{12}\text{C}^{6+}$ interacting with water as a function of the projectile’s kinetic energy T and the energy of ejected electrons W .

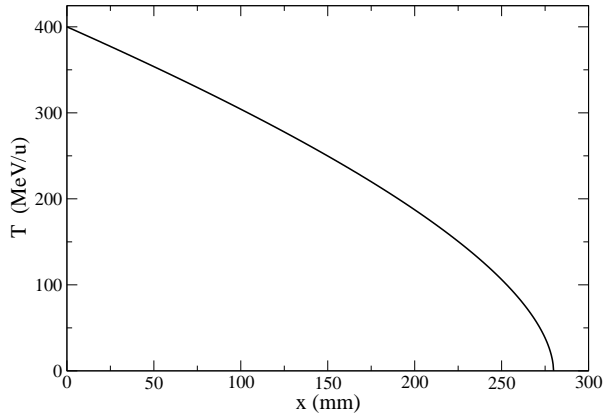


Fig. 3. Energy of $^{12}\text{C}^{6+}$ ions as a function of the penetration depth in water. The initial ion energy is 400 MeV per nucleon.

within an ion’s trajectory segment, dx :

$$\frac{dT}{dx} = -n\sigma_{st}(T) . \tag{13}$$

This quantity is known as the linear energy transfer (LET), one of the most important quantities in radiation biology. The LET found from Eq. (13) is a function of the kinetic energy of the ion rather than the ion’s position along

the path in the medium. The dependence of LET (and other quantities) on this position, however, is more suitable for cancer therapy applications. Integrating inverse LET, given by (13), we get

$$x(T) = \int_T^{T_0} \frac{dT'}{|dT'/dx|} , \tag{14}$$

where T_0 is the initial energy of the projectile. We obtain the correspondence between the position of the ion along the path and its energy. The dependence $x(T)$ for carbon ions is shown in Fig. 3.

This figure helps to remap all quantities of interest so that they depend on x rather than on T . The depth dependence of the average LET as a function of x is shown in Fig. 4. In this figure, our calculated LET is compared with the predictions of the MCHIT model [8,9,10] based on the GEANT4 toolkit [11,12]. The Monte Carlo calculations were performed both with and without taking into account nuclear fragmentation reactions. Experimental data by Schardt *et al.* [16] are also shown for comparison. Our calculated position of the Bragg peak is about 5 mm (2%) deeper than predicted by simulations and observed by the experiment. This discrepancy arises from neglecting the projectile energy loss due to non-ionization processes when the energy is spent for the excitation of neutral atoms without ejection of electrons. Indeed, it is estimated [17] as 5-15% of the total projectile energy loss.

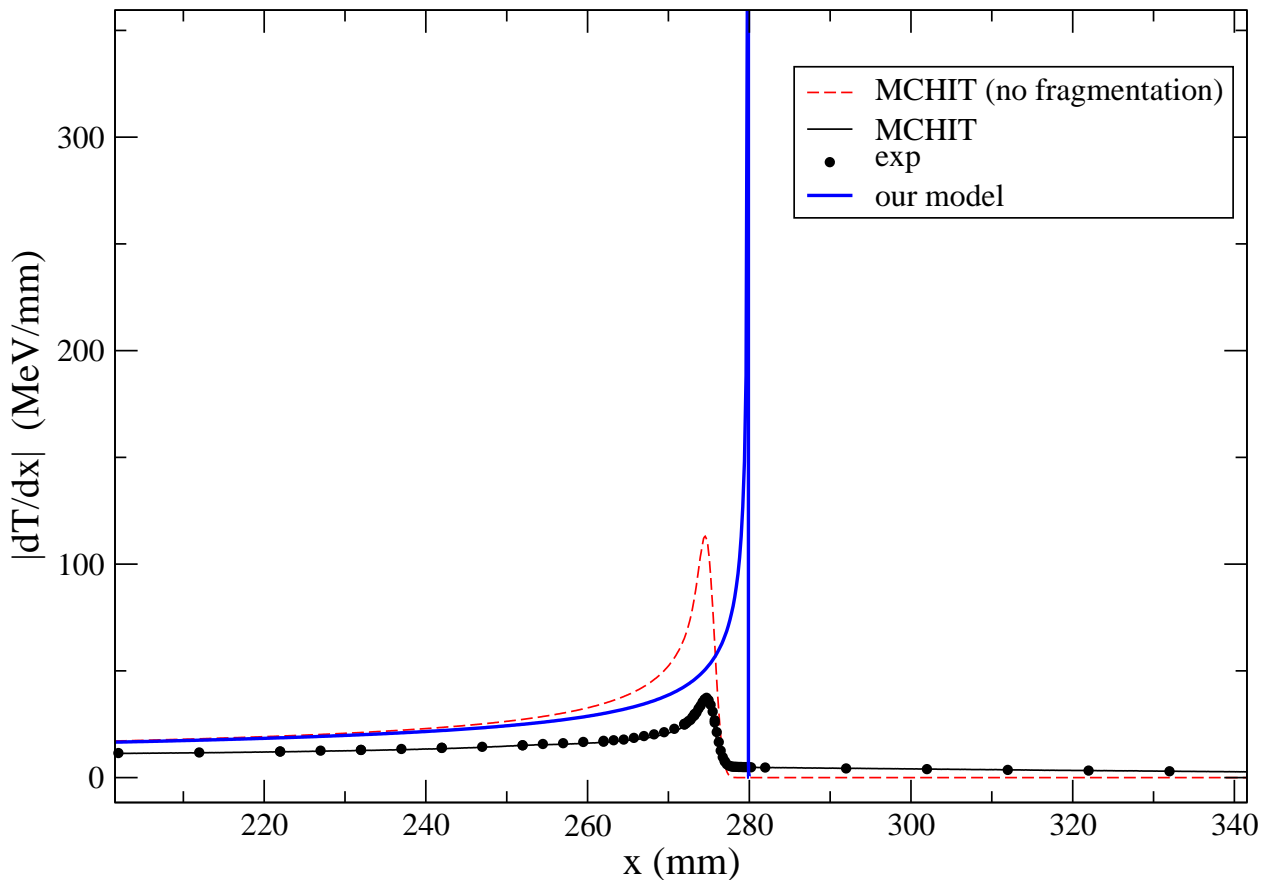


Fig. 4. Linear energy transfer of 400 MeV/u $^{12}\text{C}^{6+}$ ions as a function of penetration depth in water. The MCHIT results with and without nuclear fragmentation are shown for comparison. Points - experimental data [16]

So far our consideration neglects the fact that the projectile energy loss is a stochastic process, and $|dT/dx|$ was calculated as the average LET. Therefore, we introduced the energy-loss straggling which essentially improves the agreement with the MCHIT results obtained taking into account the stochastics of energy-loss process. In calculating the energy-loss straggling, we followed the prescription of a semi-analytical model described in Ref. [21],

$$\left\langle \frac{dT}{dx}(x) \right\rangle = \frac{1}{\sigma_{str} \sqrt{2\pi}} \int_0^{x_0} \frac{dT}{dx}(x') \exp\left(-\frac{(x' - x)^2}{2\sigma_{str}^2}\right) dx', \quad (15)$$

where x_0 is a maximum penetration depth of the projectile, and $\sigma_{str} = 0.8$ mm is the longitudinal-straggling standard deviation computed by Hollmark *et al.* [22], for a carbon ion of that range of energy. The results are presented in Fig. 5. In order to facilitate the comparison of our analytical model with MCHIT, in Fig. 5, MCHIT results are presented without taking into account nuclear fragmentation reactions, and our data are plotted with a proper shift in x , accounting for the difference between the peak positions. This allows us to consider separately the effects of electromagnetic interactions of beam nuclei.

As confirmed by MCHIT simulations [19], nuclear fragmentation reactions become important for heavy-nuclei beams and deeply-located tumors. For example, both experimental data [16] and MCHIT calculations [20] indicate that more than 40% of primary 200 MeV/u $^{12}\text{C}^{6+}$ nuclei undergo fragmentation before they reach the Bragg peak position, and this fraction exceeds 70% for 400 MeV/u $^{12}\text{C}^{6+}$ beam.

What are the effects of nuclear reactions? First, the beam is attenuated since ions are leaving the beam. Second, new projectiles are formed and they may have different penetration depths than the original carbon ions. Most important, protons and α -particles, which dominate the secondary products of such reactions [16] have much longer penetration depths at the same energy (per nucleon). This results in a substantial tail after the Bragg peak shown in Fig. 4.

The next quantity of interest is the number of secondary electrons with kinetic energy W , produced by a single ion on the interval Δx at the depth x corresponding to a certain kinetic energy T of the ion. This quantity is a product of the remapping of Eq. (1) integrated over solid angle; it can be written as follows:

$$\frac{dN(W, x)}{dW} = n \Delta x \frac{d\sigma(W, x)}{dW}. \quad (16)$$

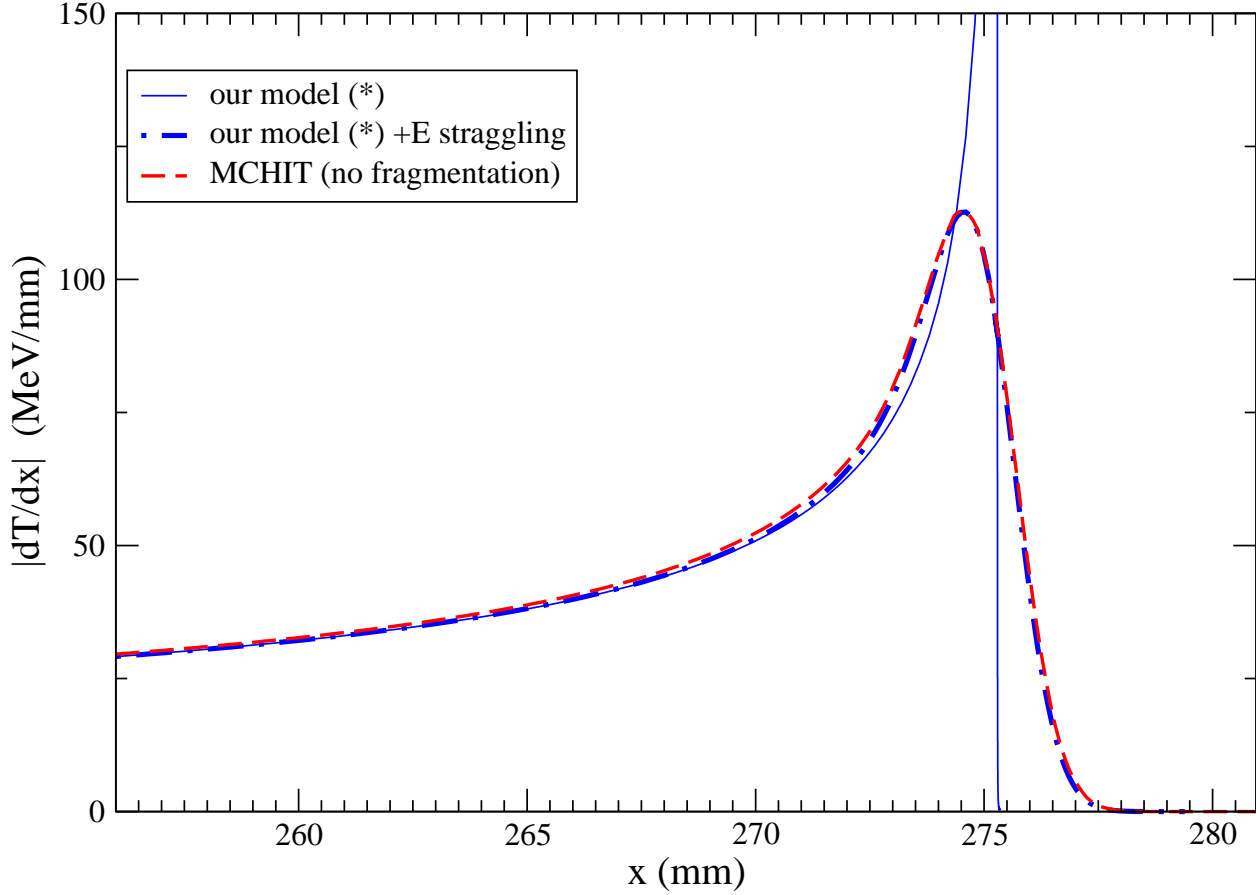


Fig. 5. Linear energy transfer of 400 MeV/u $^{12}\text{C}^{6+}$ ions as a function of penetration depth in water with and without straggling compared with the MCHIT results without nuclear fragmentation. (*)Our results are shifted by 4.6 mm for convenience in comparing the peak shapes.

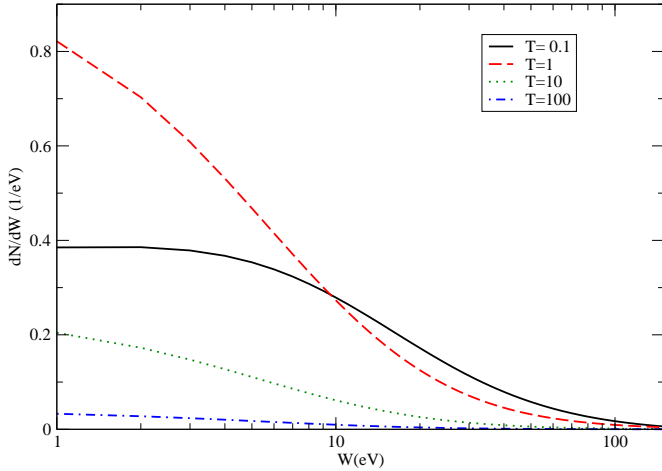


Fig. 6. Number of secondary electrons with kinetic energy W , produced by a single ion in a 1-nm interval vs. kinetic energy of the secondary electrons, for different ion's energies T (MeV/u)

Four curves shown in Fig. 6 show this dependence at different energies or depths of the ion. This number, however, represents only the secondary electrons produced by the projectile. In order to determine the total number of elec-

trons in the avalanche, one has to analyze the ionizing capabilities of these secondary electrons.

To address this issue, we calculate the fraction of secondary electrons with energies higher than the threshold of ionization produced in a single collision.

$$\phi_i = \frac{1}{\sigma(T)} \int_{I_i}^{\infty} \frac{d\sigma(W', T)}{dW'} dW' . \quad (17)$$

The dependencies for different electronic shells are shown in Fig. 7. These results are somewhat surprising since they indicate that the fraction of secondary electrons capable of further ionization decreases with increasing energy of the ion. This is probably a result of averaging; even though higher-energetic secondary electrons are produced, there are many more lower-energy ones (see Fig. 1). The fraction of secondary electrons capable of further ionization is substantial for secondary electrons produced by the projectile, even at relatively low projectile energies; however, secondary electrons produced by *secondary* electrons are even less energetic, so that further ionizations are much less probable. This is supported by calculations using Rudd's model for incident electrons. However, it can also be explained by a simple estimate: Fig. 2 indicates that the average energy of secondary electrons in the vicinity of the

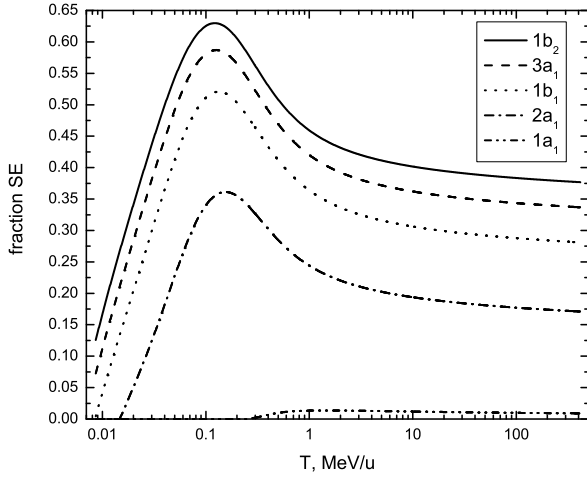


Fig. 7. Fraction of secondary electrons produced by $^{12}\text{C}^{6+}$ capable of further ionization. Different lines indicate different electronic shells of the water molecule.

Bragg peak is about 45 eV. The maximum average energy that can be transferred to the next generation secondary electron is just $(45 - I_i)/2$, which is just over 12 eV for the outermost electron, an energy barely enough to cause further ionization. Therefore, we conclude that there is no avalanche of secondary electrons and that Eq. (16) gives a reasonable estimate of the number of secondary electrons, within a factor of 2. Thus, we have analyzed the track of a single ion: we obtained the LET (depicting the Bragg peak, its shape and position), we obtained the energy spectrum of the secondary electrons, and we estimated the avalanche effects related with ionization caused by secondary electrons.

3 Direct consequences of ionization and DNA damage

In this section we estimate three components that contribute to the DNA damage: an electron plasma, free radicals produced as a result of ionization of water molecules, and heating of the medium caused by ion passage.

3.1 Electron plasma and free radicals

Let us estimate the number density of the electron plasma produced by an ion. In Section 2, we found the secondary electron energy spectrum and estimated the effect of further ionization. In order to deduce the density of the electron plasma, we have to estimate the volume occupied by these electrons. The crucial quantity for this estimate is the penetration length of the secondary electrons caused by the projectile. In principle, this estimate can be done in the same fashion as it was done for the ions in the previous section; however, the energies of the secondary electrons

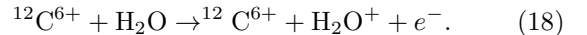
are such that Rudd’s analysis may not be reliable [15]. Therefore, we will try to rely on other available sources.

Direct experimental observations of penetration depths of electrons in liquid water are scarce. There are values recommended by the International Commission on Radiation Units and Measurements for 10 – 1000 keV electrons [23,24], and there are data for thermalization lengths of “subexcitation electrons” for lower energies, 0 – 4 eV [25]. However, there is a gap in experimental data for electron energies, which are the most interesting from the viewpoint of cancer therapy applications.

The average energy of secondary electrons in the Bragg peak area ($T \sim 0.3$ MeV per nucleon) is about 45 eV (see Fig. 2). Even though there are no direct experimental values for the penetration lengths of electrons in this energy range, interpolation of existing experimental data points [26] and theoretical predictions based on Monte-Carlo simulations [27] suggest that the penetration lengths of such electrons are of the order of 10 nm or less. Comparison of these lengths and typical distances between the ions in the beam leads us to conclude that under realistic conditions ion tracks do not interact. That is, every ion acts independently and the total biological effect equals the sum of the damages from individual ions, and therefore the collective action of ions in the beam can be neglected.

In order to get realistic order of magnitude estimates, we assume that the energy deposited by an ion is thermalized within a tube of a radius $r \sim 10$ nm.

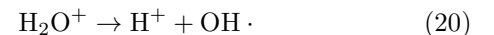
The total ionization cross section for carbon ions $^{12}\text{C}^{6+}$ of kinetic energy $T \sim 0.3$ MeV per nucleon is about $\sigma \approx 40 \cdot 10^{-16} \text{ cm}^2 = 0.4 \text{ nm}^2$. The majority of secondary electrons are produced in the following process:



The number of electrons produced per one nm of the ion’s trajectory is then $n\sigma = 33 \text{ nm}^{-3} \times 0.4 \text{ nm}^2 \approx 13 \text{ nm}^{-1}$. This quantity is easily translated into the number density of the electron plasma,

$$n_e = \frac{n\sigma}{\pi r^2} \approx \frac{13 \text{ nm}^{-1}}{\pi 100 \text{ nm}^2} \approx 0.045 \text{ nm}^{-3} = 0.45 \cdot 10^{20} \text{ cm}^{-3} . \quad (19)$$

Both secondary electrons and ionized water molecules react to form free radicals



This means that the induced concentrations of free radicals can be of the same order as the concentration of the electron plasma.

OH radicals play an important role in damaging DNA. They interact with nucleobases damaging them; moreover, “secondary” free radicals may result from these interactions [7]. Further analysis is needed in order to obtain quantitative estimates of the yields of DSB’s and other types of irreparable DNA damage due to these effects.

3.2 Dissociative recombination by low energy electrons

Traditionally, it had been believed that non-thermalized secondary electrons can not cause any significant genotoxic damage, unless they are already solvated in water and can participate in chemical reactions of the type (21) or unless they have enough kinetic energy. The singly differentiated cross section, however, falls rapidly with energy of the ejected electron and therefore energetic secondary electrons are not abundant, cf. Figs. 1 and 2.

In 2000, Sanche *et al.* [28] argued that 1- to 20-eV secondary electrons “induce substantial yields of single- and double-strand breaks in DNA, which are caused by rapid decays of transient molecular resonances localized on the DNA’s basic components” [28]. In their experiments, a monoenergetic electron beam at various incident energies was used to irradiate solid DNA samples. They observed that one electron out of 1000 – 2000 (depending on the electron energy) induced a single strand break and one electron out of 5000 – 10000 induced a DSB of a DNA molecule [29].

This type of experiment, however, can not be directly related to the problem of DNA damage induced by ions. The difference is in the density of free electrons. In Sanche’s experiments the electron density was of the order of 10^4 cm^{-3} 16 orders of magnitude lower than is created by an ion in the Bragg’s peak area, as it is estimated in the previous section.

One can nevertheless estimate the average number of electrons created in a volume occupied by one convolution of the DNA molecule. The DNA radius is about 1 nm, while the convolution (linear) length is about 4 nm, so that the volume of interest is about $V_{\text{DNA}} = 10^{-20} \text{ cm}^3$. Assuming that at least two electrons are needed in the volume of one DNA convolution to produce a double strand break, one can estimate that the required electron density

$$n_e^{\text{crit}} = \frac{2}{V_{\text{DNA}}} \approx 2 \cdot 10^{20} \text{ cm}^{-3}. \quad (22)$$

It is remarkable that such a density is of the same order of magnitude of the one that has been predicted by our simple estimates in the previous section.

3.3 Local heating

Finally, let us estimate the local heating produced in a tube of 10 nm radius by a carbon ion of 0.3 MeV per nucleon. The simplest way to do that is to use the thermodynamic equation

$$Q = \mu c \Delta T \quad (23)$$

relating the heat transferred, Q , to a system with the system’s mass μ , specific heat capacity c (4.2 J/g K for water) and the increase of system’s temperature ΔT . ΔT can then be found from the linear energy transfer $Q/\Delta x$ (typical value for ^{12}C ions is $100 \text{ MeV/mm} = 1.6 \cdot 10^{10} \text{ J/cm}$

in the Bragg peak region), the tube’s radius r and the density of water $\rho = 1 \text{ g/cm}^{-3}$:

$$Q = \rho \pi r^2 \Delta x c \Delta T, \quad (24)$$

$$\Delta T = \frac{Q/\Delta x}{\rho \pi r^2 c}. \quad (25)$$

Substituting the numerical values, one obtains $\Delta T \sim 10K$ for $r = 10 \text{ nm}$ and for the lower estimate of the tube’s radius, $r = 3 \text{ nm}$, we find $\Delta T \sim 100K$.

This estimate shows that the local heating within the electron thermalization radius along the ion track can be quite substantial. The melting temperature of a DNA molecule is about 85° C . Therefore, in our opinion, there is a need for a more thorough study of the local heating mechanism which would include investigation of such problems as the detailed description of the thermalization of secondary electrons in water, heat transfer in water, and modeling of DNA dynamics under local heating. To the best of our knowledge, this local heating mechanism has not yet received any attention.

4 Conclusions

We have presented an approach to modeling ion-beam therapy having considered the effects initiated by an energetic projectile such as a carbon ion incident on biological tissue (represented by liquid water). We analyzed passage of the ion through this medium taking into account the main processes that cause energy loss by the projectile. We succeeded in making quantitative predictions of effects such as the energy spectrum and abundance of secondary electrons and local heating caused by the projectile. Then we built our estimates of DNA damage on these predictions. In principle, the final estimates may be related to the energy deposition by the projectiles, but the microscopic analysis of the whole scenario is vitally important in order to provide more accurate predictions that may eventually contribute to the protocol of cancer therapy. Then they can be formulated into the language of dosages, energies, radiation rates, *etc.* Before that, more research is needed in understanding the mechanisms of DNA damage on a microscopic level and relating these mechanisms to the physical parameters of secondary electrons and free radicals produced by the ion beam.

Acknowledgments

This work is partially supported by the European Commission within the Network of Excellence project EXCELL and by the EU project PECU. E.S. is grateful to J.S. Payson for fruitful discussions and to FIAS for hospitality and support.

References

1. U. Amaldi, G. Kraft, *Rep. Prog. Phys.* **68**, 1861 (2005).

2. E. Pedroni, *Europhys. News* **31**, 18 (2000).
3. M. Goitein, A. Lomax, E. Pedroni, *Phys. Today* **55**, 45 (2002).
4. A. R. Smith, *Phys. Med. Biol.* **51**, R491 (2006).
5. D. T. Goodhead, *Rad. Prot. Dosim.* **122**, 13 (2006).
6. H. Nikjoo, P. O'Neill, M. Terrisol, D. T. Goodhead, *Radiat. Environ. Biophys.* **38**, 31 (1999)
7. H. Nikjoo, S. Uehara, D. Emfietzoglou, F. A. Cucinotta, *Radiat. Meas.* **41**, 1052 (2006).
8. I. Pshenichnov, I. Mishustin, W. Greiner, *Phys. Med. Biol.* **50**, 5493 (2005).
9. I. Pshenichnov, I. Mishustin, W. Greiner, *Phys. Med. Biol.* **51**, 6099 (2006).
10. I. Pshenichnov, A. Larionov, I. Mishustin, W. Greiner, *Phys. Med. Biol.* **52** 7295 (2007).
11. S. Agostinelli *et al.*, (GEANT4 Collaboration), *Nucl. Instrum. Methods A* **506**, 250 (2003).
12. J. Allison *et al.*, (GEANT4 Collaboration), *IEEE Trans. Nucl. Sci.* **53**, 270 (2006).
13. O.I. Obolensky, E. Surdutovich, I. Pshenichnov, I. Mishustin, A. V. Solov'yov, and W. Greiner, *Nucl. Inst. Meth. B*, 2008 to be published.
14. M.E. Rudd, T.V. Goffe, R.D. DuBois, L.H. Toburen, *Phys. Rev.* **A31** (1985) 492.
15. M. E. Rudd, Y.-K. Kim, D. H. Madison, T. Gay, *Rev. Mod. Phys.* **64**, 441 (1992).
16. E. Haettner, H. Iwase, D. Schardt, *Rad. Protec. Dosim.* **122**, 485 (2006).
17. G. Kraft, M. Krämer, M. Scholz, *Radiat. Environ. Biophys.* **31**, 161 (1992).
18. W. H. Barkas, *Nuclear Research Emulsions I. Techniques and Theory*, Academic Press Inc., New York, London, 1963, Vol. 1, 371.
19. I. Pshenichnov, I. Mishustin, W. Greiner, arXiv:0704.2519 [physics.med-ph], *Nucl. Inst. Meth. B*, 2008 to be published.
20. I. Pshenichnov, I. Mishustin, W. Greiner, *Towards Monte Carlo calculations of biological dose in heavy-ion therapy: modeling of nuclear fragmentation reactions*, In Proc. 2nd International Symposium "Atomic Cluster Collisions: structure and dynamics from the nuclear to the biological scale", Darmstadt, Germany, July 19 - 23, 2007, Imperial College Press, to be published
21. P. Kundrat, *Phys. Med. Biol.* **52**, 6813 (2007).
22. M. Hollmark, J. Uhrdin, D. Belkic, I. Gudowska, A. Brahme, *Phys. Med. Biol.* **49**, 3247 (2004).
23. International Commission on Radiation Units and Measurements, Bethesda, MD, *Report 37* (1984); <http://www.icru.org>.
24. M. J. Berger, J. S. Coursey, M. A. Zucker, J. Chang, National Institute of Standards and Technology, *ESTAR database*, <http://physics.nist.gov/PhysRefData/Star/Text/contents.html>.
25. V. V. Konovalov, A. M. Raitsimring, Yu. D. Tsvetkov, *Radiat. Phys. Chem.* **32**, 623 (1988).
26. D. E. Watt, *Quantities for Dosimetry of Ionizing Radiations in Liquid Water* (Taylor & Francis, London, 1996).
27. J. Meesungnoen, J.-P. Jay-Gerin, A. Filali-Mouhim, S. Mankhetkorn, *Radiat. Res.* **158**, 657 (2002).
28. B. Boudaiffa, P. Cloutier, D. Hunting, M. A. Huels, L. Sanche, *Science* **287**, 1658 (2000).
29. M. A. Huels, B. Boudaiffa, P. Cloutier, D. Hunting, L. Sanche, *JACS* **125**, 4467 (2003).

